JOURNAL OF THERMOPHYSICS AND HEAT TRANSFER
Vol. 11, No. 1, January–March 1997

Temperature Variation and Heat Transfer in Triangular Grooves with an Evaporating Film

H. B. Ma* and G. P. Peterson†
Texas A&M University, College Station, Texas 77843-3123

A mathematical model for the evaporating heat transfer coefficient and temperature variation along the axial direction of a grooved plate has been developed. The model includes the effects of the capillary-induced flow in the grooves caused by the surface tension, the two-dimensional heat conduction occurring in the wall and liquid film, and the flow and evaporation of the thin film caused by the disjoining pressure and surface tension in the thin film region. The results obtained from this model indicate that if a constant heat flux boundary condition is applied, the heat transfer coefficient will decrease and the wall temperature will increase along the axial direction. In addition, the apparent contact angle increases with increasing superheat, and hence, the heat transfer rate through the micro region also increases along the axial direction. Finally, it has been demonstrated that the contribution of the surface tension variation caused by temperature increases in the micro region can be neglected. This work will lead to a better understanding of the axial heat transfer coefficient and temperature distribution on grooved surfaces, and how these parameters affect the film thickness.

Nomenclature

A = cross-sectional area, m^2, Hamaker constant, J
a = constant
b = constant
C_1 = coefficient defined by Eq. (29)
D = diameter, m
d = top width of the groove wall, m
f = friction factor
g = gravitational acceleration, m/s^2
H = thickness of the groove wall, m
h_e = heat transfer coefficient, W/m^2 K
h_{fg} = latent heat of vaporization, kJ/kg
K = curvature, m^{-1}
k = conductivity, W/m K
L = length, m
$\dot{m}$ = mass flow rate, kg/s
p = pressure, N/m^2
p_d = disjoining pressure, N/m^2
Q = heat transfer, W
q = heat flux, W/m^2
R = gas constant, J/kg K
Re = Reynolds number
r = radius, coordinate, m
r_1 = radius defined by Eq. (21), m
r_2 = radius defined by Eq. (22), m
s = coordinate, m
T = temperature, K
U = average velocity along the axial direction, m/s
u = velocity, m/s
$\bar{u}$ = average velocity, m/s
V = volume flow rate, m^3/s
w = groove width, m
x = coordinate, m
y = coordinate, m
z = coordinate, m
α = apparent contact angle, deg
δ = film thickness, m
δ_0 = no evaporating film thickness, m
η = coordinate, m
θ = coordinate, degree
Λ = coordinate defined by Eq. (19)
μ = viscosity, Ns/m^2
ρ = density, kg/m^3
σ = surface tension, N/m
τ = shear stress, N/m^2
ϕ = half channel angle, deg
ψ = tilt angle, deg

Subscripts
c = capillary
e = evaporating
f = outside of the groove wall
h = hydraulic
in = input
j = grid number
l = liquid
lv = liquid–vapor interface
mic = micro
s = solid
sat = saturated
tot = total
v = vapor
w = wall

Received May 31, 1996; revision received Sept. 3, 1996; accepted for publication Sept. 5, 1996.

*Postdoctoral Research Associate. Member AIAA.
†Tenneco Professor and Head. Associate Fellow AIAA.

Introduction

APPLICATIONS involving micro heat pipes, mini-heat exchangers, chemical processing equipment, nuclear reactors, and thermal control systems for spacecraft, all rely upon the extremely high heat transfer rates associated with a liquid–vapor change of phase. In many of these applications, a series of small grooves is utilized to control the film thickness and provide the desired heat transfer rates. While the gravitational field and frictional flow characteristics both play an important role in the determination of the heat transfer coefficient, at very small length scales the effects of intermolecular forces such as the van der Waals force become increasingly important. A number of previous investigations[1–4] have been conducted in which the heat transfer coefficients have been determined for various geometries. For applications in-

volving grooves, the temperature and heat transfer coefficient along the axial direction has typically been assumed to be constant. Recent experimental data,[5,6] however, indicate that for both flat and curved surfaces, significant temperature variations may exist along the direction of the groove, and that assuming the value of the minimum meniscus radius at the dryout point to be zero,[7] may lead to significant errors in the estimation of the heat transfer characteristics. For these reasons, a detailed analytical investigation was conducted to determine the significance of the axial temperature variations along flat or curved, triangular micro grooves and the impact these variations could have on the heat transfer coefficient in thin film evaporation from these grooves.

The interrelationships between the evaporating heat transfer coefficient and the groove temperature, and the overall heat flux are determined by the evaporating thin film, the wall conductivity, and the capillary flow in the triangular grooves. In the current investigation, a detailed mathematical model for the evaporating heat transfer coefficient and temperature variation along the axial direction is developed that includes the effects of the capillary-induced flow in the grooves, the two-dimensional heat conduction occurring in the wall and liquid film, and the flow and evaporation of the thin film caused by the disjoining pressure and surface tension in the thin film region.

Analysis

As shown in Fig. 1, if one end of a grooved plate is immersed in a pool of liquid and held stationary at a predetermined tilt angle, the liquid will wick up the grooves against the gravitational force and the frictional force caused by continuous flow. In the current configuration, the evaporating section extends from the origin point where the grooved plate emerges from the liquid pool to the dryout point. Figure 2 shows the cross section of one triangular groove in the plate. The current analysis was performed in support of previous experimental observations[6–8] and builds upon previous theoretical analyses.[1–4,9,10] As such, it utilizes the following simplifying assumptions: 1) steady-state laminar flow in both the macro and micro regions; 2) no-slip conditions at the wall; 3) the fluid flow in the micro region is the result of gradients in the disjoining pressure, surface curvature, and surface tension; 4) the fluid flow in the macro region is the result of meniscus radius variations along the axial direction (z direction); 5) the convective terms are neglected when solving the energy equations; 6) the vapor pressure and vapor temperature are constant and saturation conditions exist in the liquid and at the interface; and 7) the radius of the liquid meniscus in the triangular grooves at a given z location is assumed constant in the macro region.

If the thermal conductivity of the plate is much larger than that of the liquid, it is reasonable to assume that there is uniform heat flux at the bottom of the grooved plate at a given z location. For convenience, it is assumed here that the heat flux through the bottom of the grooved plate is also uniform along the axial direction of the grooved plate. Again, if the conductivity of the plate is relatively high, nearly all of the heat transferred from the wall region between the grooves, to the saturated vapor region, must pass through a thin liquid film. Usually, this thin liquid film region is referred to as the micro region, and consists of the evaporating thin film region and a part of the meniscus region. Stephan and Busse[3] established a mathematical model based on the theoretical analysis presented by Wayner[11] and Wagner,[12] to calculate the heat transfer coefficient occurring in the triangular grooves, and found that the interfacial temperature variation is very important. More recently, Khrustalev and Faghri[4] developed a model based on the assumption of a constant meniscus radius, including the evaporating thin film region, in an attempt to overcome the mathematical difficulties occurring in solving the governing equation presented by Stephan and Busse.[3] However, as shown in the analysis presented by Wayner,[5] this procedure does not permit inclusion of the heat flux effects. Because the evaporating thin film profile is very important to the evaporating heat transfer and nearly all of the heat is transferred through this thin film region,[3,4] the current investigation develops a detailed dynamic mathematical model to predict the thin film profile, the heat transfer rate, the heat transfer coefficient, and the temperature variation along the axial direction of the triangular groove.

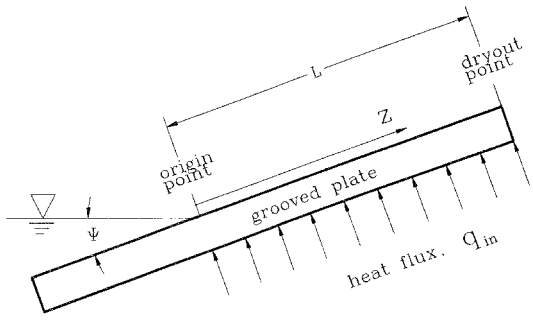

Fig. 1 Schematic of a grooved plate.

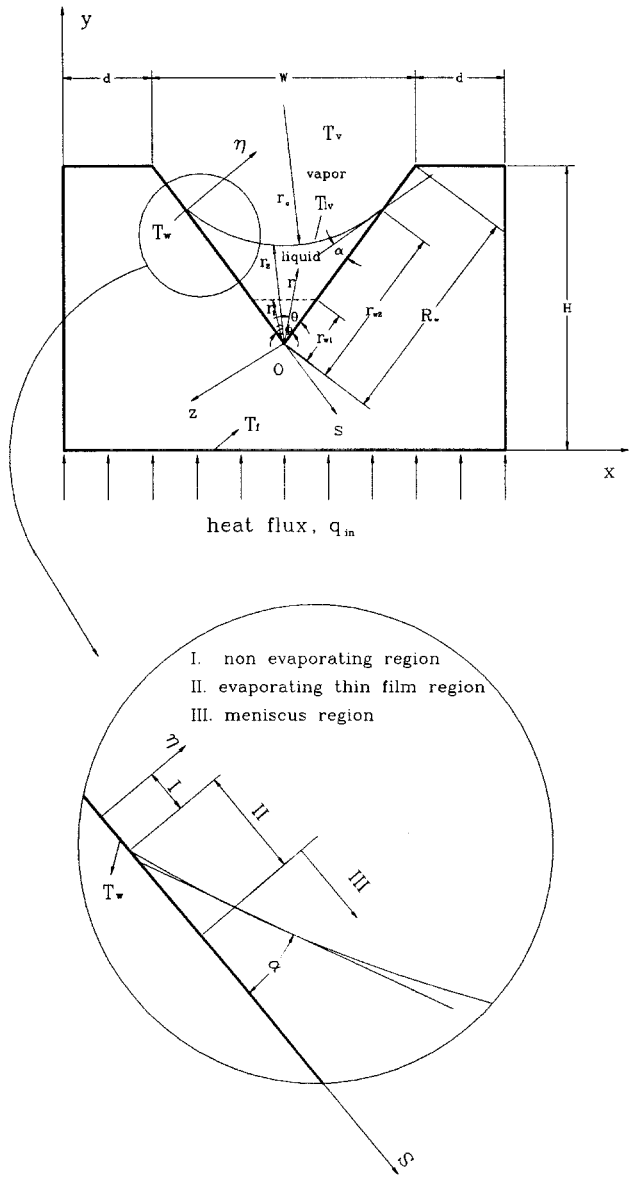

Fig. 2 Groove and liquid film.

Fluid Flow and Heat Transfer in the Evaporating Thin Film

As illustrated in Fig. 2, the liquid–vapor–solid interface consists of three regions; 1) the nonevaporating film region, where the disjoining pressure is dominant and very little evaporation takes place; 2) the evaporating thin film region, where a majority of the evaporation occurs; and 3) the meniscus region, where the meniscus radius of curvature is constant.

In the nonevaporating thin film region, the liquid–vapor interfacial temperature approaches and becomes equal to the wall temperature. Expanding the Clausius–Clapeyron equation

$$\left(\frac{dp}{dT}\right)_{sat} = \frac{h_{fg}}{T_{sat}[(1/\rho_v) - (1/\rho_l)]} \tag{1}$$

and integrating from the saturated temperature T_{sat} to the interface temperature T_{lv} results in a relationship between the interface temperature and the saturated vapor temperature[13]

$$T_{lv} = T_v[1 + (\Delta p/\rho_l h_{fg})] \tag{2}$$

where Δp can be found from

$$\Delta p = \sigma K + p_d \tag{3}$$

The first term on the right side of Eq. (3) describes the influence of the meniscus curvature K, which can be determined by

$$K = \frac{\dfrac{d^2\delta}{ds^2}}{\left[1 + \left(\dfrac{d\delta}{ds}\right)^2\right]^{3/2}} \tag{4}$$

In the second term, p_d is found by $p_d = A/\delta^3$ for nonpolar liquids and $p_d = -A/\delta^3\ \ell n(\delta/\bar{\delta}_0)$ for polar liquids.[14] Because the Hamaker constant A and the reference length $\bar{\delta}_0$ both depend on the solid–liquid properties, it is difficult to accurately determine these values for polar liquids such as water. To overcome this difficulty, the relationship developed by Holm et al.[2] was utilized

$$p_d = \rho_l R T_{lv}\ \ell n(a\delta^b) \tag{5}$$

where $a = 1.5787$ and $b = 0.0243$.

In the nonevaporating film region, the influence of K can be neglected because of the absence of vaporization, and the interface temperature can be assumed to be equal to the wall temperature. Substituting Eqs. (3) and (5) into Eq. (2), the film thickness in this region can be found as

$$\delta_0 = \exp[[(T_w/T_v - 1)(h_{fg}/RT_w) - \ell n\ a]/b] \tag{6}$$

In the evaporating thin film region, the Reynolds number of the liquid flow is very small, i.e., $Re_\delta << 1$. Hence, the inertial terms can be neglected and the velocity based on the Navier–Stokes equation for a laminar liquid flow can be found as

$$u = \frac{1}{\mu_l}\left(\frac{dp_l}{ds}\right)\left(\frac{1}{2}\eta^2 - \delta\eta\right) \tag{7}$$

Integrating Eq. (7) from 0 to δ, yields

$$V = \int_0^\delta u\, d\eta = -\frac{dp_l}{ds}\frac{\delta^3}{3\mu_l} \tag{8}$$

and the average liquid flow velocity in the evaporating thin film can be found as

$$\bar{u} = \frac{V}{A_\delta} = -\frac{\delta^2}{3\mu_l}\frac{dp_l}{ds} \tag{9}$$

The friction factor and Reynolds number product for the thin film flow in this region, can be determined by

$$f \cdot Re_\delta = \frac{\tau|_{\eta=0}}{\frac{1}{2}\rho_l \bar{u}^2} \cdot \frac{\bar{u}\delta\rho_l}{\mu_l} \tag{10}$$

where $\tau|_{\eta=0}$ is the shear stress at the wall found by

$$\tau|_{\eta=0} = \mu_l \frac{\partial u}{\partial \eta}\Big|_{\eta=0} \tag{11}$$

Substituting Eqs. (8), (9), and (11) into Eq. (10), the value of the friction factor and Reynolds number product $f \cdot Re_\delta$ can be determined. The corresponding pressure drop caused by the viscous flow can be determined as

$$\frac{dp_l}{ds} = -\frac{f \cdot Re_\delta \mu_l \dot{m}_\delta(s)}{2\delta^3(s)\rho_l} \tag{12}$$

where the mass flow rate is directly related to the evaporating heat flux, i.e.,

$$\dot{m}_\delta(s) = \int_0^s \frac{q(s)}{h_{fg}}\, ds \tag{13}$$

The driving force for the flow in the evaporating thin film is composed of the capillary pressure and the disjoining pressure, or

$$\frac{dp_c}{ds} = \frac{d(K\sigma - p_d)}{ds} = \sigma\frac{dK}{ds} + K\frac{d\sigma}{ds} - \frac{dp_d}{ds} \tag{14}$$

and for steady-state evaporation of a thin film, the pumping pressure head must be equal to the summation of the pressure drops, i.e.,

$$\sigma\frac{dK}{ds} + K\frac{d\sigma}{ds} - \frac{dp_d}{ds} = -\frac{f \cdot Re_\delta \mu_l \dot{m}_\delta(s)}{2\delta^3(s)\rho_l} \tag{15}$$

Because of the property characteristics of the liquid, as the temperature increases in the direction of flow, the surface tension decreases and the temperature-induced surface shear stress, shown as the second term in Eq. (15), will hinder fluid flow toward the contact line.[15] However, for the current investigation, the contribution of this term is very small compared to the other terms, and here was found to be less than 0.4%.

The boundary conditions corresponding to Eq. (15) can be expressed as

$$\delta = \delta_0, \qquad K = 0, \qquad \frac{d\delta}{d\eta} = 0, \quad \text{at} \quad s = 0 \tag{16}$$

Heat Transfer in the Macro Region

The heat transfer passing through the wall of the groove and the liquid film shown in Fig. 2, can be described by the two-dimensional heat conduction equation

$$\nabla \cdot [k\nabla(T)] = 0 \tag{17}$$

While the temperature distribution resulting from conduction in the wall can be easily determined using a finite difference method, the irregularity of the surface of the liquid film makes use of the finite element method more attractive for this region,[3] particularly when a one-dimensional model is used to approximate it, as was the case in the model developed by Khrustalev and Faghri.[4] In the current investigation, a coordinate transformation is introduced and the irregular geometric shape can be changed into a regular one, allowing the use of the finite difference method for both regions.

The heat conduction equation shown in Eq. (17), when applied to the liquid film shown in Fig. 2, can be rewritten as

$$\frac{\partial^2 T}{\partial r^2} + \frac{1}{r}\frac{\partial T}{\partial r} + \frac{1}{r^2}\frac{\partial^2 T}{\partial \theta^2} = 0 \tag{18}$$

Applying a coordinate transformation

$$\Lambda = \ell n(r/r_1)/\ell n(r_2/r_1) \tag{19}$$

Eq. (18) becomes

$$\frac{\partial^2 T}{\partial \Lambda^2} + \frac{\partial^2 T}{\partial \theta^2}\left(\ell n \frac{r_2}{r_1}\right)^2 = 0 \tag{20}$$

where r_1 and r_2 can be determined from the following expressions:

$$r_1 = r_{w1}\frac{\cos \phi}{\cos(\phi - \theta)} \tag{21}$$

$$r_2 = r_{w2}\frac{\cos \alpha \cos(\phi - \theta) - [\sin^2\phi - \cos^2\alpha \sin(\phi - \theta)]^{0.5}}{\cos(\alpha + \phi)} \tag{22}$$

respectively. The radius r_1 in Eq. (21) is an assumption as shown in Fig. 2. When $r_1 \to 0$, the solution corresponds to that obtained for a triangular groove. Numerically, it was taken as 10^{-10} m in the current investigation. The boundary conditions corresponding to Eqs. (17) and (20) (see Fig. 2) can be expressed as

$$\frac{\partial T}{\partial y}k_s = q_{\text{in}} \quad \text{at} \quad y = 0 \tag{23}$$

$$\frac{\partial T}{\partial n} = 0 \tag{24}$$

at the dry part of the groove

$$T = T_{\text{lv}} \tag{25}$$

at the liquid–vapor interface and

$$\frac{\partial T}{\partial x} = 0 \quad \text{at} \quad x = 0, \qquad x = \frac{W}{2} + d \tag{26}$$

Capillary Flow Along the Groove

Evaporation in the thin film region requires continuous axial liquid transport in the groove where the liquid film thickness is large enough that the disjoining pressure effect can be neglected. In addition, even at the dryout point where the meniscus radius is at a minimum,[9] the disjoining pressure is small compared to the axial mass transport resulting from the capillary pressure, and only the capillary pressure need be considered. Thus, conservation of momentum for the liquid flow in the groove can be expressed as

$$\frac{\mathrm{d}}{\mathrm{d}z}\left(\frac{\sigma}{r_c}\right) = \rho_l g \sin(\psi) + \frac{2f_l \rho_l U_l^2}{D_h} \tag{27}$$

where the inertial effects are neglected compared with those caused by viscous losses.[16] The values of f_l can be found from the numerical solution of the two-dimensional momentum equation.[17]

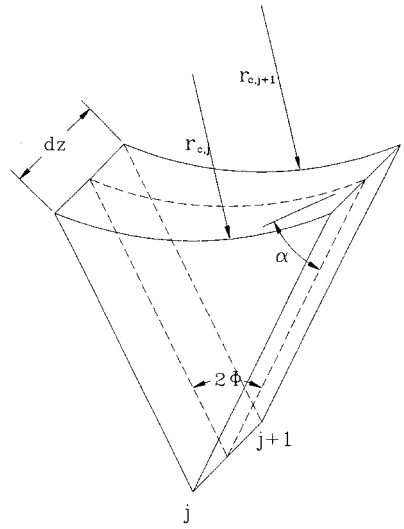

Fig. 3 Control volume.

Utilizing the control volume shown in Fig. 3, Eq. (27) takes the form[9]

$$\sigma\left(\frac{1}{r_{c,j+1}} - \frac{1}{r_{c,j}}\right) = \rho_l g(z_{j+1} - z_j)\sin \psi + \frac{(Re \cdot f)\mu_l \dot{m} \cos^2(\alpha + \phi)(r_{c,j+1} + r_{c,j})^2}{C_1^3 \sin^2\phi \rho_l (r_{c,j+1}^2 + r_{c,j}^2)^3}(z_{j+1} - z_j) \tag{28}$$

where

$$C_1 = \frac{1}{2}\int_0^{2\phi}\left\{\frac{\cos \alpha \cos(\phi - \theta) - [\sin^2\phi - \cos^2\alpha \sin^2(\phi - \theta)]^{0.5}}{\sin^2\phi}\right\}^2 \mathrm{d}\theta \tag{29}$$

Equation (28) represents one control volume within the total axial liquid flow region of the groove. Because the groove is divided into N control volumes, there are N equations, one governing each control volume. To solve the system of equations defined in Eq. (28), it is necessary to determine the boundary conditions. For the first control volume, i.e., the origin point where the grooved plate emerges from the liquid pool, as shown in Fig. 1, the meniscus radius can be found from the geometric shape by assuming a constant meniscus radius. For the last control volume, i.e., the dryout point, the capillary radius will depend on the heat flux and the balance between the shear stress and the capillary forces.

Numerical Treatment

In the current investigation, the film thickness variation and heat transfer through the thin film can be modeled using the third-order ordinary differential equation (ODE), described previously, and can be solved using a fourth-order Runge–Kutta method, which will result in a unique numerical solution. Since the heat flux, film thickness, and interface temperature are all interrelated and mutually dependent, an iterative solution technique must be used to find the heat flux distribution and film thickness variation in the micro region, where the disjoining pressure plays an important role.

The value of T_{lv} can be determined from Eq. (2). When the film thickness increases, the interface temperature decreases and approaches a constant value, i.e.,

$$T_{\text{lv}} = T_v[1 + (\sigma K/\rho_l h_{fg})] \tag{30}$$

where the disjoining pressure has a very small effect and can be neglected. The micro region model presented in this article is not suitable for those regions where the disjoining pressure

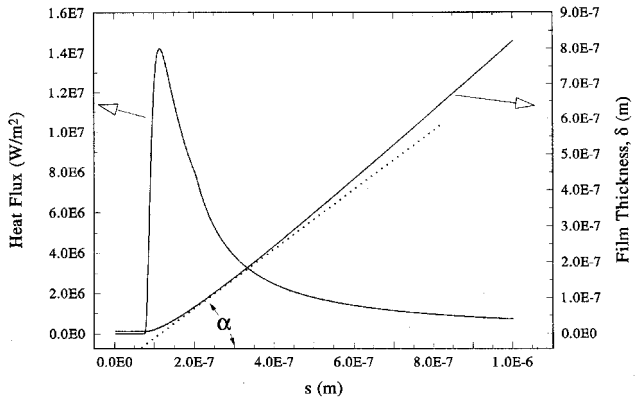

Fig. 4 Heat flux distribution and film thickness variation in the micro region ($T_w - T_v$ = 1.0 K).

has no effect and the meniscus radius of curvature approaches a constant.

Because the curvature of the liquid film in the micro region varies as a function of the angle α, shown in Fig. 4, and is defined as

$$\alpha = \arctan\left(\frac{d\delta}{ds}\right) \tag{31}$$

as the film thickness increases, α increases. With this increase in the film thickness, the disjoining pressure effect decreases and becomes so small that it can be neglected, and α approaches the apparent contact angle. Based on this contact angle, the meniscus radius of curvature and the film thickness variation in the macro region can be determined. The detailed procedure for the heat transfer coefficient and temperature distribution along the z direction is based on the following steps:

1) Solve Eq. (28) using an assumed contact angle to obtain the meniscus radius distribution along the grooves.

2) Solve Eq. (15) with an assumed wall temperature to find the heat flux rate through the thin film region, the thin film thickness profile, and the interfacial temperature variation in the thin film region using a Runge–Kutta technique.

3) Solve Eqs. (17) and (20) with the wall temperature assumed in step 2 to find the temperature distribution in the wall and macro region of the liquid film using the finite difference method with a line-by-line procedure and a combination of the tri-diagonal matrix algorithm and the Gauss–Seidel technique.

4) Calculate the heat flux through the micro and macro regions of the liquid film. If the total heat transport calculated is different from the heat flux added to the wall q_{in}, as shown in Fig. 2, go back to step 2 and repeat the procedure with a new assumed wall temperature.

5) Compare the resulting apparent contact angle with the assumed contact angle. If they are different, go back to step 1 and repeat the procedure using the new contact angle.

The effect of the step size and grid number have been investigated to ensure grid independence. Nonuniform grids were employed to capture the features induced by the coordinate transformation defined by Eq. (19). For the micro region, a step size, 5×10^{-10} m was used to solve Eq. (15) using the Runge–Kutta method. For the macro region in the solid wall, an 86 × 60 control volume grid was used to solve Eq. (17) using finite difference methods. For the macro region of the liquid film, a 120 × 100 grid was employed to find the temperature distribution.

Results and Discussion

To better illustrate the temperature variation and heat transfer in triangular grooves with an evaporating film, a triangular groove, similar to that shown in Fig. 2, with dimensions of d = 0 m, W = 0.0006 m, H = 0.0015 m, ϕ = 30 deg, L = 0.06 m, and ψ = 20 deg was analyzed using the current model and the thermophysical properties of copper and pure saturated water at 20°C. The model presented in this article can be used to predict the meniscus profile and the heat transfer rate in the micro region. As shown in Fig. 4, comparison of the film thickness (right-hand ordinate) and the heat flux (left-hand ordinate) indicates that the disjoining pressure has a significant effect on the thickness of the thin film, particularly in the evaporating thin film region. As illustrated, the heat flux is initially zero in the region where the film thickness is constant, and then increases dramatically as the film thickness enters the thin film evaporating region. As the angle defined by Eq. (31) increases along the s direction, the film meniscus approaches a nearly constant slope. And as the disjoining pressure approaches zero, the angle defined by Eq. (31) assumes an almost constant value. In the current model, the angle defined by Eq. (31), i.e., the point where the disjoining pressure becomes zero, was used to represent the apparent contact angle, and the meniscus radius of curvature was assumed to be constant with the same radius of curvature as that occurring in the macro region.

It is apparent here that the film profile and the angle defined by Eq. (31) depend on the superheat, i.e., $T_w - T_v$. As the superheat increases, the film thickness and apparent contact angle increase, as shown in Figs. 5 and 6, and the evaporating heat flux changes dramatically along the s direction, as shown in Fig. 4. As the interface temperature varies from $T_{lv} = T_w$ at s = 0, to $T_{lv} = T_v$ at the end of the region, the effect of the disjoining pressure diminishes to zero. Because the heat flux and film profile in the micro region are both dependent upon the capillary liquid flow in the macro region, i.e., along the axial direction, it is necessary to know the liquid film distribution in the axial direction. The results indicate that for a given heat flux, tilt angle, channel angle, contact angle, and

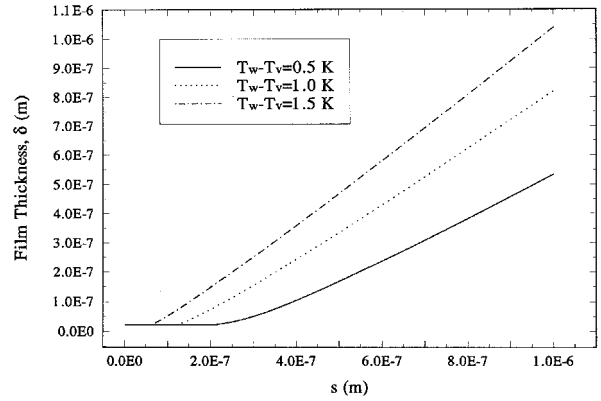

Fig. 5 Superheat effect on the film thickness variation in the micro region.

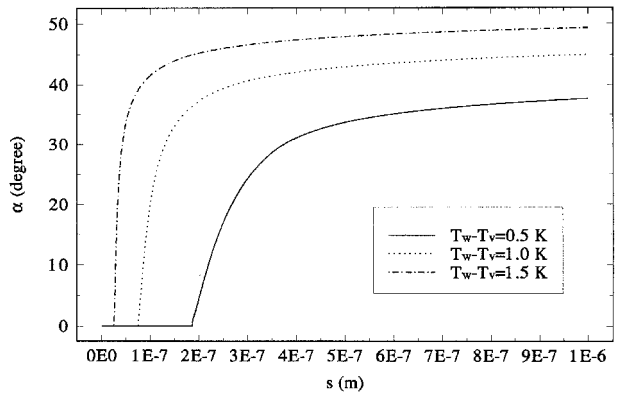

Fig. 6 Superheat effect on the apparent contact angle.

working fluid, the interaction between the evaporation and the force balance that exists between the capillary force and the pressure drop, will result in a liquid flow distributed as shown in Fig. 7. As shown in Fig. 1, the liquid has the largest capillary pressure and the largest meniscus radius at the origin point. As the liquid climbs up to the groove, the meniscus radius and the cross-sectional area of the liquid flow decrease because of the opposing force caused by friction and gravity. From Fig. 7, it can be found that the meniscus radius of curvature varies from the largest value at $z/L = 0$ to a minimum value at $z/L = 1$, and also that the cross-sectional area of liquid flow along the grooves changes dramatically from $z/L = 0$ to $z/L = 1$. Since the profile of the liquid film along the axial direction of the grooved plate varies, the temperature distribution in the liquid film and solid wall will also change. This implies that the heat transfer coefficient, defined as

$$h_e = q_{in}/(T_f - T_v) \tag{32}$$

and the heat transport ratio Q_{mic}/Q_{tot} must also vary. Here, Q_{mic} is the heat transport through the micro region, i.e., $0 < s < 10^{-6}$ m, and Q_{tot} is the heat transport through both the micro region and the macro region, and is equal to

$$Q_{tot} = q_{in}A_s \tag{33}$$

where A_s is equal to $(2d + w) \times$ unit length, as shown in Fig. 2. The different film profiles will directly affect the temperature distribution in the film and solid wall, the heat transfer coefficient, and the heat transport ratio. Because of the meniscus radius variation in the macro region along the axial direction, the superheat in the macro region will increase (although it has a very small effect on the heat transfer coefficient compared with other effects), and the interface heat resistance will increase along the axial direction. Figures 8a–8c illustrate the liquid film profile and the temperature distribution in the liquid film and solid wall for three given locations: 1) the origin point, 2) the midpoint between the origin and the dryout point, and 3) the dryout point as shown in Fig. 1.

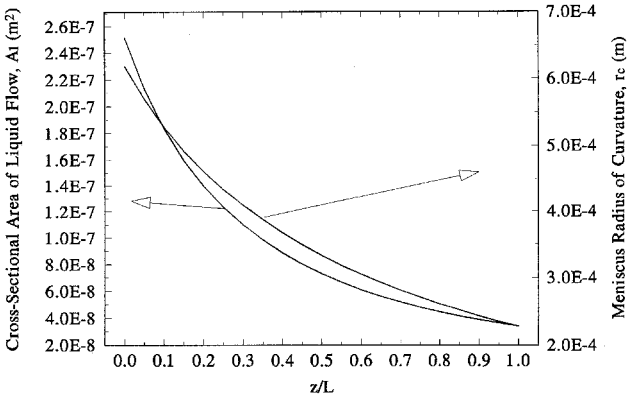

Fig. 7 Meniscus radius and cross-sectional area of liquid flow along the axial direction of a groove.

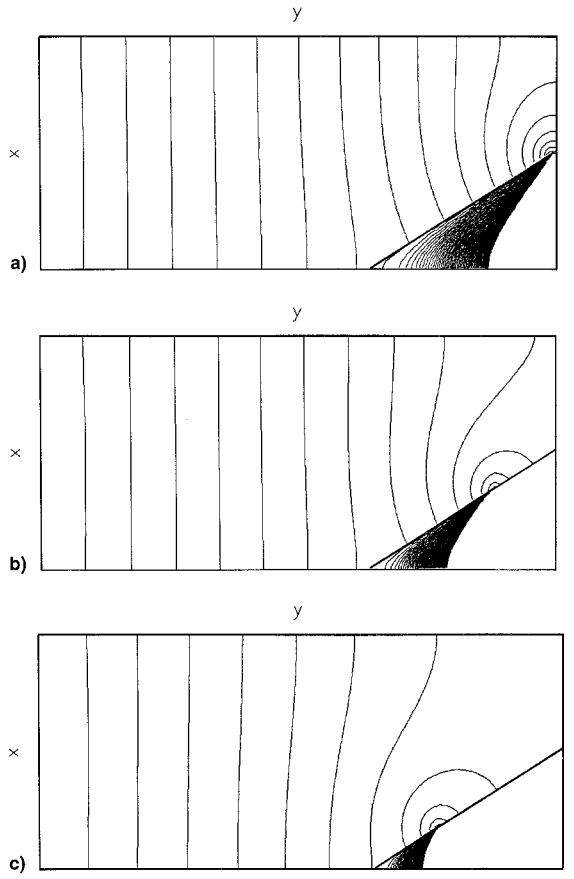

Fig. 8 Isotherms in the solid wall and liquid film (temperature difference between two isotherms: $\Delta T = 0.0042$ K) at the a) origin point, b) midpoint between the origin and the dryout point; and c) dryout point.

As the liquid climbs up the groove, the cross-sectional area, i.e., the wetted area, decreases, and the heat transport through the macro region will also decrease. Since the boundary condition is one of constant heat flux, the total heat transport is constant. As a result, the heat transport through the micro region will increase. Figure 9 illustrates quantitatively the heat transport ratio variation along the axial direction. As shown, Q_{mix}/Q_{tot} increases from 21.7% at $z/L = 0$ to 44.9% at $z/L = 1$ for the example examined here. The increase in heat transport in the micro region requires an increase of the wall temperature in the micro region, i.e., T_w, or $T_w - T_v$, and will result in an increase in the apparent contact angle as shown in Fig. 6. The detailed variation of the apparent contact angle along the axial direction can be found in Fig. 9. Because of the increases in both the heat transport through the micro region and the wall temperature, the outer wall temperature T_f, will increase, as shown in Fig. 10. Since the heat flux and vapor temperature are assumed to be constant, the heat transfer coefficient defined by Eq. (32) will decrease along the axial direction of the grooved plate. From Fig. 10, it can be found that the heat transfer coefficient will change from 6.7 W/cm^2 K at $z/L = 0$ to 3.7 W/cm^2 K at $z/L = 1$ for the current example.

To verify the model presented herein, results obtained using the current model were compared with the numerical data reported by Stephan and Busse,[3] and Khrustalev and Faghri,[4] and the model developed by Schneider et al.[18] and Shekriladze and Rusishvili[19] using the following properties and geometry: $T_v = 300$ K, $K_s = 221$ W/(m^2 K), $W = 0.001$ m, $H = 0.0015$ m,

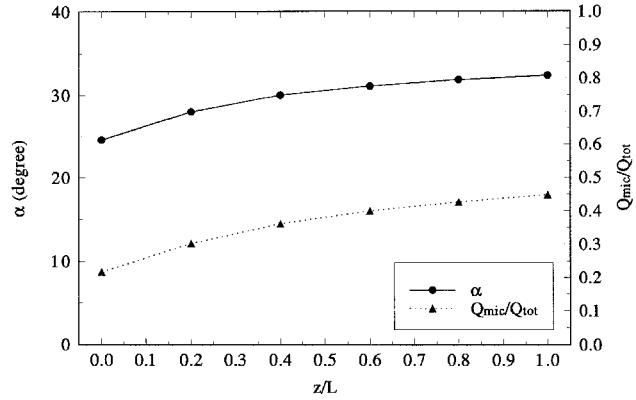

Fig. 9 Apparent contact angle and heat transport ratio along the axial direction of the groove.

Table 1 Comparison of the calculated results with the previous models

	Present article	Ref. 4	Ref. 3		Ref. 9	Ref. 18
Parameters	$T_{lv} > T_v$	$T_{lv} > T_v$	$T_{lv} > T_v$	$T_{lv} = T_v$	$T_{lv} = T_v$	$T_{lv} = T_v$
$T_f - T_v$, K	1.31[a]	1.31[a,b]	1.31[a]		—	—
h_e, W/cm^2 K	1.34–1.78[a]	1.74,[b] 2.39[a]	2.3[a]	7.9[a]	3.9[a]	6.9[a]
q_{in}, W/cm^2	1.75–2.34[a]	2.56,[b] 3.69[a]	3.0[a]	10.4[a]	—	—
Q_{mic}/Q_{tot}, %	19.4–42.0[a]	3.7[b], 38[a]	45[a]	94[a]	—	—

[a]Smooth surface. [b]Rough surface.

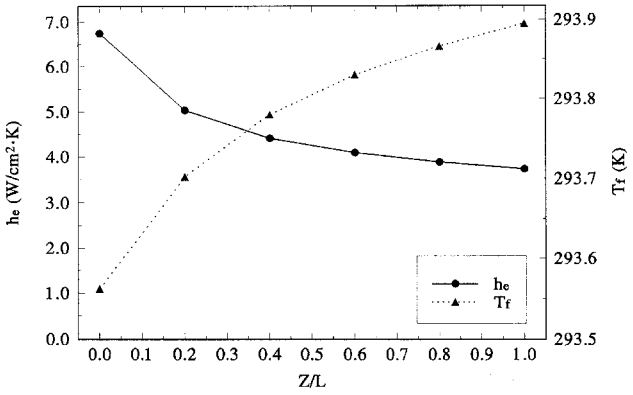

Fig. 10 Heat transfer coefficient and outer wall temperature along the axial direction of the groove.

ϕ = 45 deg, d = 0 m, and $T_w - T_v$ = 1.31 K. The detailed results of this comparison are listed in Table 1 and demonstrate the validity of the current investigation. Schneider et al.[18] and Shekriladze and Rusishvili[19] both assumed that the interfacial temperature was equal to the vapor temperature and obtained the heat transfer coefficient. Stephan and Busse[3] noticed that the interfacial temperature variation is very important and should not be assumed to be equal to the vapor temperature because of the surface curvature and disjoining pressure effect. More recently, Khrustalev and Faghri[4] found that the governing equation developed by Stephan and Busse[3] was difficult to solve, and developed a model based on the assumption of a constant meniscus radius.

While helpful in understanding the physical effects, none of these models can predict the heat transfer coefficient variation or the temperature distribution along the axial direction of the grooved plate. It is clear, however, that the liquid film profile and the ratio Q_{mic}/Q_{tot} vary along the axial direction as shown previously, and hence, will result in the variations of both the heat transfer coefficient and temperature along the axial direction, as shown in the experimental investigations.[6,8,20] However, because these experimental investigations did not examine the detailed temperature distribution and the heat transfer coefficient variation along the axial direction, they cannot be explicitly compared with the results obtained here. The trend, however, is similar. For example, the average heat transfer coefficient obtained by Ivanovskii et al.[20] was equal to 0.95 W/cm^2 K, which is close to the value predicted here. To accurately verify the model presented in this article, it is necessary to establish a new experimental system to verify the detailed heat transfer coefficient variation and temperature distribution along the axial direction in the triangular groove.

Conclusions

A detailed mathematical model for predicting the heat transfer coefficient and temperature variation along the axial direction of a grooved plate has been developed that includes the effects of the capillary-induced flow in the grooves caused by the surface tension; the two-dimension heat conduction occurring in the wall and liquid film; and the flow and evaporation of the thin film caused by the disjoining pressure and surface tension in the thin film region. In this model, the governing equation for the liquid flow in the micro region has been reduced to a third-order ODE that was solved using a fourth-order Runge–Kutta method to yield a unique solution. Applying the coordinate transformation, the irregular shape of the liquid film was transformed into a regular shape, which can be easily solved using a finite difference method. In this way, the governing equations for the heat transfer and liquid flow in both the micro region and macro region were solved to obtain a solution for this three-dimensional problem that includes the effects of the capillary pressure, disjoining pressure, surface tension, gravity, frictional force, and irregular-shape boundary conditions.

The results obtained from this model indicate that if a constant heat flux boundary condition exists, the heat transfer coefficient will decrease and the wall temperature will increase along the axial direction. In addition, the apparent contact angle increases with increasing superheat, and hence, the heat transfer through the micro region also increases along the axial direction. Finally, it has been demonstrated that the contribution of the surface tension variation as a result of the temperature increases in the micro region can be neglected. This work will lead to a better understanding of the heat transfer coefficient and temperature distribution along the axial direction of these types of grooved plates, and how these parameters affect the film thickness and the resulting heat transfer coefficient.

References

[1]Kamotani, Y., "Evaporator Film Coefficients of Grooved Heat Pipes," *Proceedings of the 3rd International Heat Pipe Conference*, Stanford Press, Palo Alto, CA, 1978, pp. 128–130.

[2]Holm, F. W., and Goplen, S. P., "Heat Transfer in the Meniscus Thin Film Transition Region," *Journal of Heat Transfer*, Vol. 101, No. 3, 1979, pp. 543–547.

[3]Stephan, P. C., and Busse, C. A., "Analysis of the Heat Transfer Coefficient of Grooved Heat Pipe Evaporator Walls," *International Journal of Heat and Mass Transfer*, Vol. 35, No. 2, 1993, pp. 383–391.

[4]Khrustalev D., and Faghri, A., "Heat Transfer During Evaporation on Capillary-Grooved Structures of Heat Pipes," *Journal of Heat Transfer*, Vol. 117, No. 3, 1992, pp. 740–747.

[5]Wayner, P. C., "Thermal and Mechanical Effects in the Spreading of a Liquid Film Due to a Change in the Apparent Finite Contact Angle," *Journal of Heat Transfer*, Vol. 117, No. 4, 1994, pp. 938–945.

[6]Xu, X., and Carey, Y. P., "Film Evaporation from a Micro-Grooved Surface — An Approximate Heat Transfer Model and Its Comparison with Experimental Data," *Journal of Thermophysics and Heat Transfer*, Vol. 4, No. 4, 1990, pp. 512–520.

[7]Ha, J. M., and Peterson, G. P., "The Interline Heat Transfer of Evaporating Thin Film Along a Micro Grooved Surface," American Society of Mechanical Engineers, Paper 95-WA/HT-20, Nov. 1995.

[8]Ma, H. B., and Peterson, G. P., "Experimental Investigation of the Maximum Heat Transport in Triangular Grooves," *Journal of Heat Transfer*, Vol. 118, No. 3, 1996, pp. 740–746.

[9]Peterson, G. P., and Ma, H. B., "The Theoretical Analysis of the Maximum Heat Transport in Triangular Grooves — A Study of Idealized Micro Heat Pipes," *Journal of Heat Transfer*, Vol. 118, No. 3, 1996, pp. 731–739.

[10]Peterson, G. P., "Modeling, Fabrication and Testing of Micro Heat Pipes: An Update," *Applied Mechanics Review*, Vol. 49, No. 4, Pt. 2, 1996, pp. 113–117.

[11]Wayner, P. C., Kao, Y. K., and LaCroix, L. V., "The Interline Heat Transfer Coefficient of an Evaporating Wetting Film," *International Journal of Heat and Mass Transfer*, Vol. 19, No. 3, 1976, pp. 487–492.

[12]Wayner, P. C., "Adsorption and Capillary Condensation at the Contact Line in Change of Phase Heat Transfer," *International Journal of Heat and Mass Transfer*, Vol. 25, No. 4, 1982, pp. 707–713.

[13]Mirzamoghadam, A., and Catton, I., "A Physical Model of the Evaporating Meniscus," *Journal of Heat Transfer*, Vol. 110, No. 1, 1988, pp. 201–207.

[14]Darjauin, B. V., and Zorin, Z. M., "Optical Study of the Absorption and Surface Condensation of Vapors in the Vicinity of Saturation on a Smooth Surface," *Proceedings of the 2nd International Congress on Surface Activity*, Vol. 2, Butterworths, London, 1957, pp. 145–152.

[15]Wayner, P. C., Tung, C. Y., Tirumala, M., and Yang, J. H., "Experimental Study of Evaporation in the Contact Line Region of a Thin Film of Hexane," *Journal of Heat Transfer*, Vol. 107, No. 1, 1985, pp. 182–189.

[16]Khrustalev, D., and Faghri, A., "Thermal Analysis of a Micro Heat Pipes," *Journal of Heat Transfer*, Vol. 116, No. 2, 1994, pp. 189–198.

[17]Ma, H. B., and Peterson, G. P., "The Influence of Vapor-Liquid Interactions on the Liquid Pressure Drop in Triangular Microgrooves," *International Journal of Heat and Mass Transfer*, Vol. 37, No. 15, 1994, pp. 2211–2219.

[18]Schneider, G. E., Yovanovich, M. M., and Wehrle, V. A., "Thermal Analysis of Trapezoidal Grooved Heat Pipe Evaporator Walls," AIAA Paper 76-481, Jan. 1976.

[19]Shekriladze, I. G., and Rusishvili, D. G., "Evaporation and Condensation on Grooved Capillary Surface," *Proceedings of the 6th International Heat Pipe Conference*, Vol. 2, Ja Tech Publishing, Tsukuba, Japan, 1987, pp. 77–82.

[20]Ivanovskii, M. N., Privezentsev, V. V., Il'in, Y. A., and Sidorenko, E. M., "Experimental Investigation of Heat Transfer with Evaporation of the Agent from a Corrugated Capillary Structure," *Journal of Engineering Physics and Thermophysics*, Vol. 46, No. 4, 1984, pp. 377–381.